

# A microbead array chemical sensor using capillary-based sample introduction: toward the development of an “electronic tongue”

Young-Soo Sohn<sup>a,\*</sup>, Adrian Goodey<sup>b</sup>, Eric V. Anslyn<sup>b</sup>, John T. McDevitt<sup>b</sup>,  
Jason B. Shear<sup>b</sup>, Dean P. Neikirk<sup>a</sup>

<sup>a</sup> The University of Texas at Austin, Department of Electrical and Computer Engineering, Austin, TX 78712, USA

<sup>b</sup> The University of Texas at Austin, Department of Chemistry and Biochemistry, Austin, TX 78712, USA

Received 12 June 2004; received in revised form 27 August 2004; accepted 27 August 2004

Available online 2 December 2004

## Abstract

The development of a micromachined fluidic structure for the introduction of liquid samples into a chip-based sensor array composed of individually addressable polymeric microbeads is presented. The micromachined structure consists of micromachined storage cavities combined with a covering glass layer that confines the microbeads and fluidic channels. In our sensor array transduction occurs via optical (colorimetric and fluorescence) changes to receptors and indicator molecules that are covalently attached to termination sites on the polymeric microbeads. Spectral data are acquired for each of the individual microbeads using a charged-coupled device (CCD) allowing for the near-real-time analysis of liquid sample. Hence the micromachined fluidic structure must allow for both optical access to the microbeads and fluid flow through the micromachined cavities that serve as the microreactors/analysis chambers. One of the key parts of the structure is a passive fluid introduction system driven only by capillary force. This simple means of fluid introduction realizes a compact device. The capillary flow on the inlet channel has been studied, and the responses of the microbeads (alizarin complexone) to a liquid sample have been characterized. The test results show that this system is useful in a micro-total-analysis-system ( $\mu$ -TAS) and biomedical applications.

© 2004 Elsevier B.V. All rights reserved.

**Keywords:** Chemical sensor array; Microbeads; Microfluidic; Capillary; Micromachine

## 1. Introduction

The development of smart sensors with chemical and biological responses has become increasingly important for medical, environmental, military, and industrial processing applications. Various types of bio- and chemical sensors have been developed for such applications (Abe et al., 1979; Johnson et al., 1988; Lee et al., 1994; Kondoh and Shiokawa, 1995; Kang et al., 1997; Michael et al., 1998; Eaton et al., 2004; Lotierzo et al., 2004). The developments of receptors,

detection principles, and device fabrication techniques are all-important factors in the success of these chemical and biological detection systems (Sohn et al., 2000).

Technical and economic factors both affect the development of the microfluidic devices involved in these types of sensors. The motivations and advantages include reduced initial sample volume, the minimal usage of expensive reagents, increased functionality and parallelism in sample analysis resulting in faster analysis time, compact size, and low cost. A wide range of device architectures and material choices has been adapted for various applications of interest (Kugelmass et al., 1999). Though plastic materials have gained more and more attention since they have a wide range of material properties at low cost and can be micromachined in a variety of manners, the silicon micromachining technology that integrated such microfluidic devices with microelectronics is

\* Corresponding author. Present address: The University of Texas at Austin, J.J. Pickle Research Campus, 10100 Burnet Road, Bldg. #160, MER 1.604A, R9900, Austin, TX 78758, USA. Tel.: +1 512 471 6707 (O)/+1 512 791 1896 (M); fax: +1 512 471 8575.

E-mail address: [sohn.js@mail.utexas.edu](mailto:sohn.js@mail.utexas.edu) (Y.-S. Sohn).

still an attractive approach (Petersen, 1996; Baltes, 1997; Büttgenbach and Robohm, 1998; deMello, 2002).

Combinatorial arrays of chemical sensors have also been synthesized to address a wide variety of analyses, thereby enabling the investigation of a large number of possible molecule interactions in parallel (Kovacs, 1998). Sensor arrays that function as electronic noses have been developed for the identification and quantification of vapors (Gardner and Bartlett, 1994). However, for many important applications, such as medical and beverage processing, a solution-phase analysis is desired without requiring the decomposition of the analytes (Savoy et al., 1998).

The sensations of smell and taste results from a series of specific and nonspecific molecular recognition events that take place in parallel. In a few cases there are receptors that are specific for individual analytes. However, most tastants and odorants are identified through a composite of responses from nonspecific interactions. The pattern created by the simultaneous response of these receptors is specific for a particular set of stimuli. A series of chemically active sites, taste buds, are located within depressions in the tongue where the molecular and ionic analytes become restricted to allow time for their identification. These taste buds can respond to the five primary taste: sweet (carbohydrate based), sour (acidity), salty (ionic), umami (savory or meaty), and bitter (quinine and other alkaloids). Combining the magnitude of these five signals, along with olfactory information, creates a distinct pattern for each tastant. The pattern is analyzed by the brain, remembered, and recognized later as a specific tastant. The “electronic taste” chip developed by The University of Texas researchers mimic many of the features exhibited by the human sense of taste. Polymer microbeads were derivatized with a variety of receptors and indicator molecules to mimic taste buds, and the microbeads were positioned within micromachined cavities localized on a silicon chip to mimic the cavities in which natural taste buds reside. Multianalyte mixtures can be analyzed and intelligent decisions related to chemical composition of solution-phase samples can be made rapidly and accurately with the new detection modality. Data streams were acquired for each of the individual beads. The resulting patterns were stored in a computer and used for the

simultaneous identification and quantification of multiple analytes in solution. This sensor array, electronic tongue, has the similar ability to be exposed to new analytes, learn what patterns represent, store them, and recall them for future reference (Lavigne et al., 1998; Savoy et al., 1998; Goodey et al., 2001).

This paper presents the design, fabrication, and testing of a new sample introduction system for an integrated micromachined sensor array that can allow the rapid characterization of multi-component mixtures in a solution. The sensor uses an array composed of microbeads in micromachined cavities localized on silicon wafer. Sensing occurs via colorimetric and fluorescence changes to receptors and indicator molecules that are attached to termination sites on the polymeric microbeads. As a result, the sensor array system enables simultaneous and near-real-time analyses using small samples and reagent volumes with the capacity to incorporate significant redundancies, so that false signals can be recognized in contrast to real signals (Lavigne et al., 1998; Savoy et al., 1998; Goodey et al., 2001). One of the key parts of the system discussed in this paper is a passive pump driven only by capillary force. The hydrophilic surface of the fluidic structure draws the sample into the sensor array without any moving mechanical parts. Since there is no moving mechanical component in the structure, the size of the fluidic structure can be compact and the fabrication becomes simple when compared to the device including active microfluidic components. These factors should make the proposed system inexpensive to mass-produce, portable and compatible with biomedical applications.

## 2. The background chemistry results

Although the design, assembly and characterization of sensor array systems capable of identifying in near-real-time the presence of complex mixtures of analytes represent an ambitious goal, a number of important experiments have already been completed demonstrating the feasibility and utility of our array system. Each of the following items has already been accomplished:

Table 1  
Current taste chip analyte summary

Analyte	Class	Sample matrix	Assay type	Visualization methods	Status
H(+)	pH	Aqueous	pH indicator	Colorimetric, fluorescence	Optimized, fully tested, compared with standards, ANN studies
Ca(+2), Mg(+2)	Electrolyte	Aqueous	Compleximetric indicator	Colorimetric	Optimized, fully tested
Glucose	Sugar	Aqueous	Enzyme assay	Colorimetric, fluorescence	Optimized, fully tested
ATP, GTP, AMP	Biological cofactor	Aqueous	Dye displacement assay	Fluorescence	Optimized, fully tested, PC studies
CRP	Protein, cardiac risk factor	Human serum, saliva	Immunology	Colorimetric, fluorescence	Optimized, fully tested, compared with standards
IL-6	Cytokine	Human serum, saliva	Immunology	Colorimetric, fluorescence	Proof of principle
DNA oligos	Generic tests	Aqueous	Hybridization	Fluorescence	Optimized, fully tested

1. An impressive range of detection capabilities extending across multiple analyte classes have been adapted to the bead-array platform. Derivatization of polymer beads with both colorimetric and fluorescent dye layers. These structures have been shown to give patterns that are selective for to pH,  $\text{Ca}^{2+}$ , simple sugars,  $\text{F}^-$  and  $\text{La}^{3+}$ , DNA, proteins, biological cofactors, and toxins (see Table 1).
2. Favorable comparisons between the analytical characteristics derived from our platform and the macroscopic “gold standard” methods have been established and published for the areas of pH, metal cation, cardiac risk factor and DNA oligonucleotide detection.
3. Reversible and sensitive sensing with response times well less than 1 min (typically on the order of seconds) have been accomplished with the bead sensors.
4. Micromachined arrays suitable both for confinement of the artificial “taste buds” as well as optical characterization have been prepared. These structures allow for the rapid introduction of the test fluids while allowing spectrophotometric and fluorescence assays to probe the analyte concentration.
5. Integration of the test bed arrays with commercially available CCD detectors has been accomplished. Data streams for red–green–blue channels have been recorded for a variety of bead structures.
6. Polymer bead structures having optical properties suitable for both transmission and fluorescence assays have been identified. Compatibility with aqueous environments for the polymer beads used here is important for the rapid diffusion of analyte species into the active sites of the individual sensor structures.
7. Fluorescence images and optical absorption measurements show that the dyemodified beads localized within the micromachined arrays display optical properties similar to those obtained for the same dye when dissolved freely in solution.
8. A number of effective methods for creating oligomeric structures capable of binding biologically relevant groups have been developed.
9. Incorporation of simple dyes into beads that possess receptors has been demonstrated, leading to “smart dyes” with optical responses to the presence of the correct analyte.

Table 1 summarizes the analytes that have been successfully detected in our current micromachined platform (Lavigne et al., 1998; Curey et al., 2001; Goodey et al., 2001; Christodoulides et al., 2002; McCleskey et al., 2003; Park et al., 2003; Ali et al., 2003).

### 3. Microbeads and micromachined sensing platform

Sensing is based on the optical changes that occur in receptors and indicator molecules attached to the polymeric

microbeads that are typically a few hundred micrometers in diameter. The microbeads are located in a pre-set arrangement of micromachined cavities. The resulting optical signatures form a pattern that can be identified and quantified using Image Pro Plus 4.0 software (Media Cybernetics, Silver Spring, MD, USA) on a workstation. Since signal transduction is accomplished by the analysis of the optical (absorbance for colorimetric detection and fluorescence) signals from the microbeads, optical access through the microfluidic structure is required, as illustrated in Fig. 1a. An optical

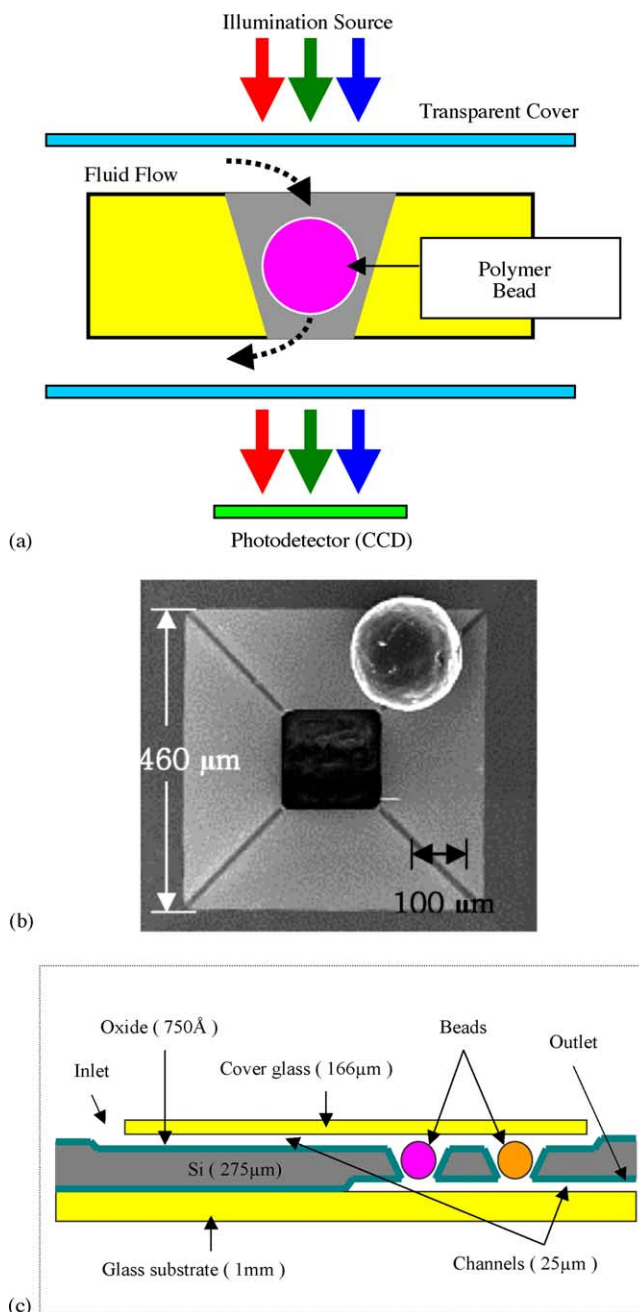


Fig. 1. (a) Optical detection and data analysis systems. (b) Scanning electron micrograph of the micromachined cavity and a polymer bead. (c) Cross-sectional view of the microfluidic structure.

illumination source, a white light for colorimetric measurement, is positioned above or below the micromachined device, and an illuminating light then passes through the micromachined device to reach the optical detectors, typically CCD.

Microbeads have been widely used since they are convenient solid phase supports for receptors, have good optical properties, and can be easily and inexpensively acquired with diameters values in the range of 120–350  $\mu\text{m}$ . With the use of these microbeads it is possible to utilize an effective sampling thickness up to 350  $\mu\text{m}$ . This long effective path length combined with large flow rate has the potential to lower detection thresholds and increase measurement sensitivity for the microbead array methods relative to other array strategies that exploit monolayer films or thin polymeric pads (Arenkov et al., 2000; Goodey et al., 2001). Bead material choice is based on the method of derivatization and also for its compatibility with aqueous solution. Typical materials for the microbeads are polystyrene–polyethylene glycol (small molecule, anions, cations) and agarose (enzymes, proteins, antibodies) (Bodanszky, 1993; Lavigne et al., 1998; Goodey et al., 2001). Some microbead materials swell when exposed to organic and aqueous fluids. Under typical analysis conditions,  $\sim 85\%$  of the internal environment of the microbead is composed of solvent. A light cross-linking of the matrix backbone provides good mechanical properties to these systems as well as restoring force that fosters the reversible exchange of solvents in to and out of the microbeads (Goodey et al., 2001). To take advantage of polymer swelling with keeping the beads in proper location we have chosen to use a confining structure (micromachined cavities) designed to allow for the expansion of the microbead while avoiding problems incurred by attaching the polymer to platform and providing an undisturbed optical path through the microbeads and allowing for fluid flow through the micromachined cavities which serves as reaction and analysis chambers. A scanning electron micrograph of the micromachined cavity and a polymer bead is shown in Fig. 1b.

Aptamers and unnatural biopolymers can be used immediately in a sensing mode simply by attaching the receptors to a bead that is already derivatized with a dye sensitive to its microenvironment. Therefore, the signaling protocol becomes routine and does not have to be engineered each and every time, only the receptors need to be engineered (Savoy et al., 1998). Batches of beads can be individually and independently prepared. Additionally, instrumentation and robotics for measuring and manipulating these beads are commercially available (Quantum Dot Corporation (QDC), <http://www.qdots.com/live/index.asp>). The products of Quantum Dot Corporation (QDC)<sup>TM</sup> and BioSphere Medical<sup>TM</sup> (BioSphere Medical, <http://www.biospheremed.com/index.cfm>) using these microbeads (microspheres) are on the market in medical applications and research laboratories (Xu et al., 2003).

#### 4. Device fabrication

Fig. 1c shows a cross-sectional view of the fluidic structure. The basic structure consists of three layers: the cover glass, the micromachined silicon and the glass substrate. The cover glass is used to prevent the microbeads from escaping from their individual micromachined cavities without any optical obstruction and to channel the sample fluid flow. The silicon is etched twice, firstly, to form the micromachined cavities that support the microbeads and secondly, to form the flow channels. The glass substrate allows optical access and provides mechanical stabilization for the silicon substrate.

In order to protect the characteristics of the receptors and indicator molecules from heat and chemicals during the chip fabrication, an appropriate fabrication sequence must be used. Fig. 2 shows a schematic diagram of the fabrication procedure. A lightly doped, double side polished 4 in. single crystal  $\langle 100 \rangle$  silicon wafer with 275  $\mu\text{m}$  thickness was used as the substrate. Anisotropic wet chemical etching has been used to fabricate the micromachined cavities and channels in the single silicon substrate. A silicon nitride ( $\text{Si}_3\text{N}_4$ ) layer deposited by LPCVD was used as mask layer for the bulk etch. A  $10 \times 10$  array of squares ( $460 \mu\text{m} \times 460 \mu\text{m}$ , center-to-center spacing of  $610 \mu\text{m}$ ) was patterned on the silicon wafer (Fig. 2a), and the silicon was anisotropically etched to form the cavities (Fig. 2b). Timed-etch stop was used to control the channel depth. The sizes of the top channel and bottom channel were  $25 \text{ mm} \times 8 \text{ mm}$  and  $10 \text{ mm} \times 8 \text{ mm}$ , respectively. During channel etching, the change in the shape of the micromachined cavities was negligible since the typical values for the selectivity of  $\langle 100 \rangle$  over  $\langle 111 \rangle$  in planes in KOH etchants is 300–400 (Kovacs, 1998). The channel

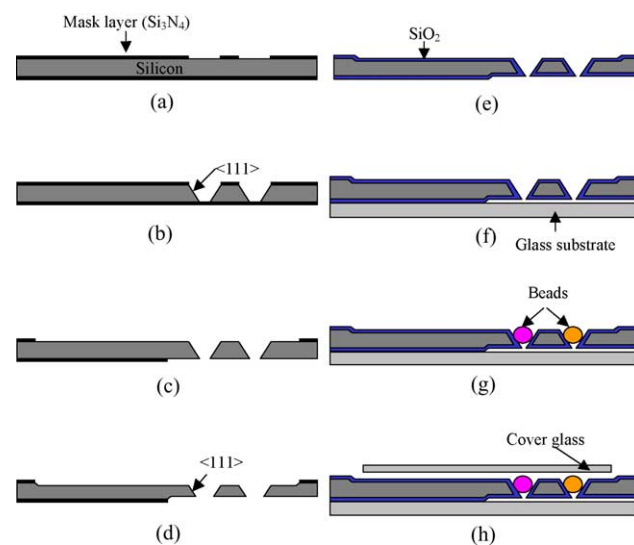


Fig. 2. Schematic diagram of fabrication procedure of the microfluidic device. (a) Pattern for the array of etch cavities. (b) Etching of silicon by KOH solution. (c) Patterns for the channels on both sides. (d) Etching for the channels on both sides. (e) Removal of the mask layer and deposition of silicon dioxide ( $\text{SiO}_2$ ) layer. (f) Attachment to glass substrate by bonding. (g) Placement of the beads in the etch cavities. (h) Application of cover glass.

depth created by micromachining was about 25  $\mu\text{m}$  (Fig. 2c and d). After all silicon micromachining was completed, a silicon dioxide ( $\text{SiO}_2$ ) layer was deposited using the LPCVD process in order to enhance surface wetting for sample introduction (i.e., to ensure that the chip surfaces are hydrophilic) (Fig. 2e). After the silicon substrate fabrication was completed, it was bonded to the glass substrate using anodic bonding (Fig. 2f). The glass substrate used in this fabrication was BOROFLOAT™ flat glass (US Precision Glass, Elgin, IL, USA). BOROFLOAT™ flat glass is highly resistant to water, neutral, acidic, and saline solutions, as well as to chlorine, bromine, iodine, and organic substances. The linear thermal coefficient of expansion of BOROFLOAT™ flat glass is close to that of silicon. Therefore, any stress due to the difference in the thermal expansion coefficients of the two substrates become small. The glass substrate and the micromachined silicon were bonded at about 260 °C with a constant high voltage (1000 V) with the anode on the silicon. After the micromachined silicon substrate was attached to the glass substrate, each microbead was placed in the etch cavities using a pick-and-place tool to form the sensor array (Fig. 2g). The outlet of the micromachined silicon was connected to a vacuum, which then sucked the beads towards it when a bead approached a micromachined cavity. Here, a tungsten tip and probe used in electronic probe stations were used. Finally, the cover glass was attached to the rest of the device using a UV curable adhesive (Fig. 2h). The cover glass used in this fabrication was a microscope cover glass with a thickness of 165  $\mu\text{m}$ .

## 5. Results and discussion

### 5.1. Horizontal capillary and fluid flow

A number of previous devices have used surface tension to transport liquids without the need of any moving mechanical parts; such forces are considered to be dominant in the microdomain (Went, 1968; Kim, 2000). In our device, a horizontal capillary has been utilized to introduce the sample fluid; for such a system, one quantity of interest is the velocity of the fluid front  $v$  (i.e., the velocity of the leading liquid–air interface as the sample is first drawn into the system). In order to study the impact of inlet channel dimension on this velocity, one can start with fluidic resistance defined as the ratio of pressure drop over flow rate, analogous to electrical resistance,

$$R = \frac{\Delta P}{Q}, \quad (1)$$

where  $\Delta P$  is the pressure difference in  $\text{N/m}^2$ , and  $Q$  is the volume flow rate in  $\text{m}^3/\text{s}$  (Kovacs, 1998); here

$$Q = whv. \quad (2)$$

For the device, a rectangular cross-section is assumed with top channel depth ( $h = 25 \times 10^{-6} \text{ m}$ ), and width ( $w = 8 \times 10^{-3} \text{ m}$ ) that is much larger than the depth. The capillary pressure is assumed to be the only driving force for fluid transport. The capillary pressure for a rectangular cross-section channel can be calculated from Eq. (3)

$$\Delta P = \gamma \cos \theta 2 \left( \frac{1}{h} + \frac{1}{w} \right), \quad (3)$$

where  $\theta$  is the contact angle and  $\gamma$  is the surface tension in  $\text{N/m}$ . Using the fact that  $w \gg h$ , Eq. (3) becomes

$$\Delta P \cong \frac{2\gamma}{h} \cos \theta, \quad (4)$$

and the fluidic resistance for rectangular channels with width much larger than depth is approximately (Kovacs, 1998)

$$R = \frac{12\mu L}{wh^3}, \quad (5)$$

where  $\mu$  is the viscosity of the sample fluid in  $\text{kg}/(\text{m s})$ , and  $L$  is the channel length in  $\text{m}$ . When Eqs. (2), (4) and (5) are

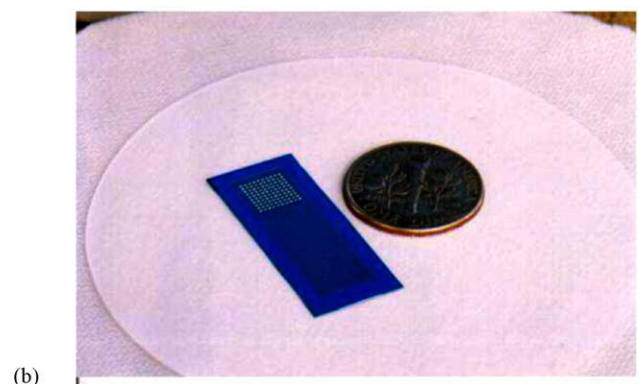
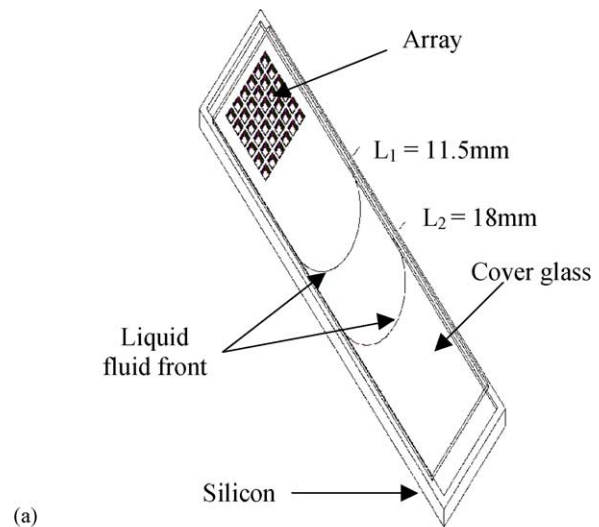


Fig. 3. (a) A three-dimensional scheme of the microfluidic device with the corresponding dimensions. (b) Microphotograph of the micromachined silicon device.

substituted into Eq. (1), the velocity of penetration can be obtained, and is given by

$$v = \frac{dL}{dt} = \frac{\gamma h}{6\mu L} \cos \theta. \quad (6)$$

Eq. (6) is quite similar to the Washburn equation calculated for a pipe with a circular cross-section having uniform radius (Washburn, 1921). To more directly compare with actual measurements, Eq. (6) can be integrated with respect to length and time

$$\int_{L_1}^{L_2} L dL = \frac{\gamma h}{6\mu} \cos \theta \int_{t_1}^{t_2} dt, \quad (7)$$

where  $L_1$  is the length of sample inlet channel that has been filled with liquid at time  $t_1$ , and  $L_2$  is the length of sample inlet channel that has been filled with liquid at time  $t_2$ . Eq. (7) then yields

$$\cos \theta = \frac{3\mu}{\gamma h} \frac{L_2^2 - L_1^2}{t_2 - t_1}. \quad (8)$$

When water, test fluid, was first introduced to our device, observation of the fluid flow front yields approximate values for  $L_1$ ,  $t_1$ ,  $L_2$ , and  $t_2$ . Typical values for the introduction of water were  $L_1 = 11.5$  mm,  $L_2 = 18$  mm,  $t_2 - t_1 = 0.333$  s. Assuming the surface tension ( $\gamma$ ) is 0.073 N/m for air/water at 20 °C and

1 atm (White, 1986), then Eq. (8) gives a contact angle of approximately 20°. There is, however, experimental uncertainty in the absolute length the liquid front has traveled as a function of time; error propagation through Eq. (8) suggests that a change in length of about 5% would yield a contact angle of approximately 0°. For water and a contact angle of 0° (characteristic of the highly hydrophilic oxide surface), Eq. (6) predicts a velocity at 14.75 mm into the channel of 20.6 mm/s, that compares well with the observed velocity at this point of 20 mm/s. Fig. 3 shows a three-dimensional scheme of the microfluidic device with the corresponding dimensions and a microphotograph of the fabricated microfluidic device.

As the fluid reaches the end of the capillary inlet channel and approaches the array area, one general trend was observed for many different devices: the sample fluid (DI-water) always flows completely around the array and into the spaces between the individual cavities before the fluid reaches the end of the top channel and begins to flow into the cavities themselves. This may be caused by the loss of driving source, surface tension, above the micromachined cavities. Hence, the fluid flows easily around the array and into the spaces between the cavities, which is similar to the electrical current that prefers to flow in a way that is less resistive. This is illustrated by Fig. 4, showing how the sample fluid, DI-water, flows through the system. Typically the water front nears the

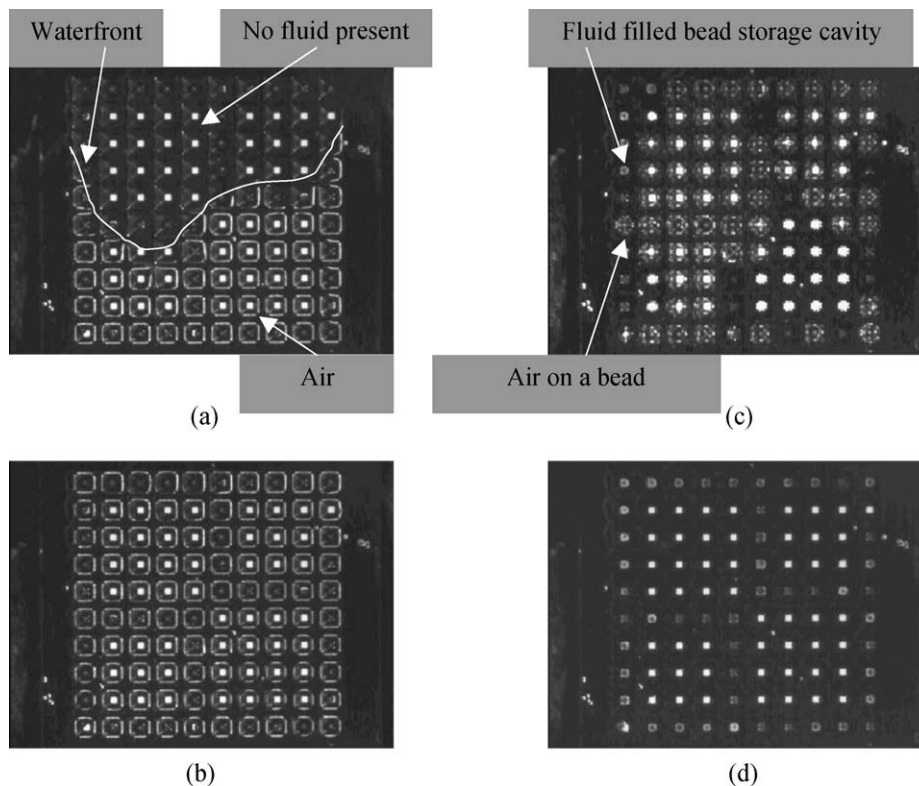


Fig. 4. Photomicrographs of a water sample as it flows through the chip. (a) Waterfront approaches the cavities and the water passes around and between the cavities, with bubbles clearly seen in the cavities themselves. (b) The water has passed completely around and between all the cavities, but at this point all the wells are still filled by air-bubbles. (c) The water flows into the cavities and the order in which the air-bubbles in the cavities disappear varies from chip to chip, and does not seem to be strongly correlated with physical location in the array. (d) All the cavities have been filled with the water, and all air-bubbles have disappeared.

end of the capillary introduction stage and reaches the micro-machined bead storage cavities approximately 3 s after the water was first placed at the inlet of the chip. Fig. 4a shows the system at  $t = 3.6$  s, as the water passes around and between the cavities, with air clearly seen in the cavities themselves. Fig. 4b shows the system at  $t = 4$  s, showing that the water has passed completely around and between all the cavities, but at this point all the cavities are still filled by air. Fig. 4c shows the system at  $t = 4.5$  s as flow begins into the cavities. The flows of the fluid in the cavities are slightly different from each cavity and from chip to chip. The average velocities of fluid flowing through the cavities were spread in the range from  $40.9 \mu\text{m/s}$  (latest) to  $107.1 \mu\text{m/s}$  (earliest), which was measured from the captured movie frames. This randomness is probably due to slightly different surface effects across the micromachined array generated during the chip fabrication. Another trend is that fluid in a cavity that reaches the bottom earlier waits for fluid in the other cavities to arrive at the bottoms of the cavities since the fluid encounters an abrupt change in geometry at the bottom of cavity (from small to large) for a hydrophilic surface. When all fluid in the cavities arrives at the bottoms in the array a positive pressure from the top (inertia) pushes the fluid to pass through the bottom of the cavities. Similarly if material property of a channel is hydrophobic (contact angle  $\theta > 90^\circ$ ) and the liquid fluid flows from larger cross-sectional area to smaller cross-sectional area, additional pressure is required to force the fluid from a wider channel to a narrower channel. Therefore, these structures can function as a stop valve (Puntambekar et al., 2002; Feng et al., 2003). Finally at  $t = 10$  s (Fig. 4d) all the cavities have been filled and air has totally disappeared.

### 5.2. The response of microbeads to the sample fluid

To more quantitatively characterize the time domain fluid flow through actual sensing beads, microbeads sensitive to the sample fluid were used. Indicator molecules attached to the microbeads were alizarin complexone, and the sample fluid was a pH 1 HCl solution. Fig. 5a shows typical graphs of red, green and blue transmitted light intensities for an alizarin bead as the pH 1 HCl solution moves through the chip. The intensities were initially constant and then changed slightly for a short time as the fluid flowed across the cover glass over the beads. At some point in time that was slightly different for each bead, the R–G–B transmitted light intensity begins to change, and finally results in an overall color change in the beads from purple (before sample introduction) to orange (after complete response to the pH 1 solution). Fig. 5a also shows the intensities of two different alizarin beads that react to the same solution to confirm the reproducibility. There is slight difference between two RGB intensities. However, this minute variation can be turned into a negligible quantity by applying to Beer's law to get absorbance values which is parameter of interest. For colorimetric detection schemes, three 'effective absorbance' values are determined by Beer's law (Eqs. (9)–(11)), using the RGB color intensities of an

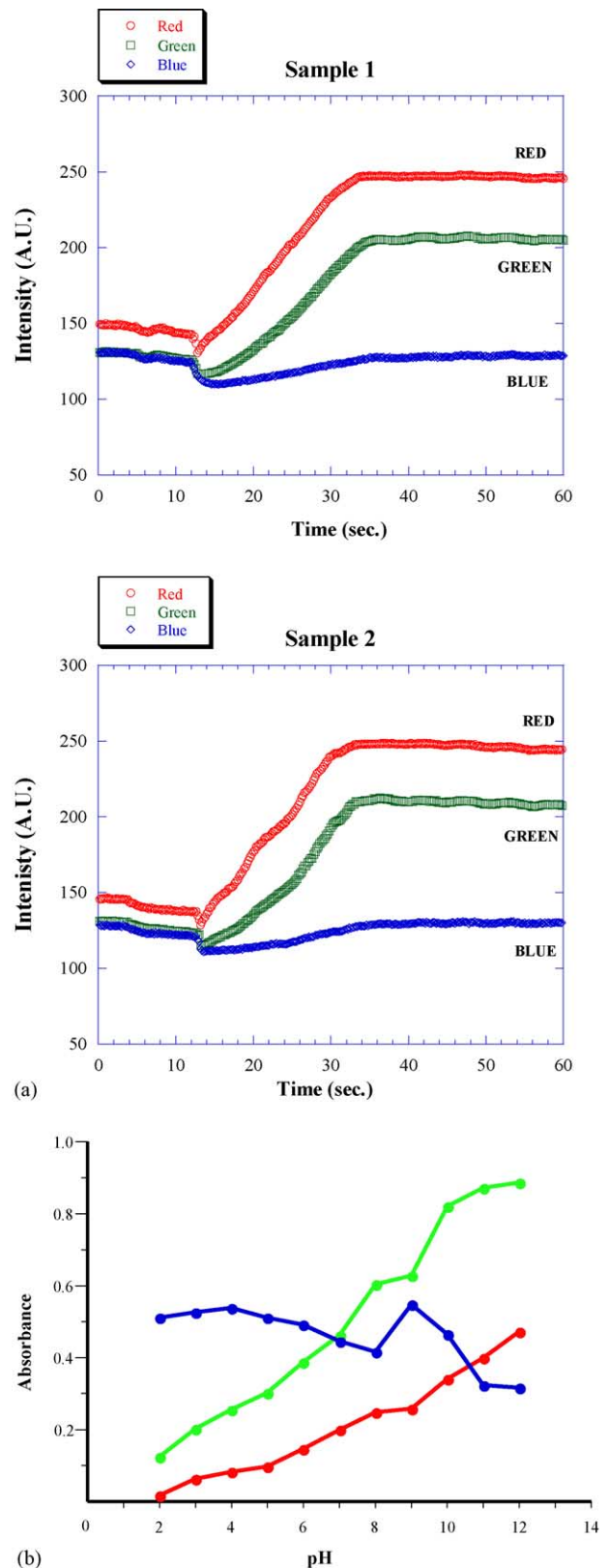
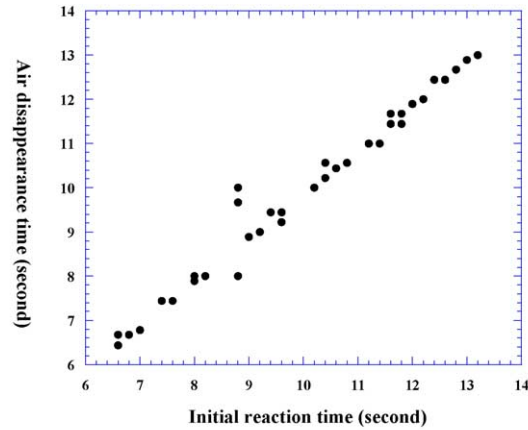


Fig. 5. (a) Change in transmitted light intensity for alizarin beads as a pH 1 HCl test solution is pulled through the chip by capillary force. (b) Absorbance values of the alizarin complexone beads as the pH is varied over the range of 2–12 using basic sensing scheme in one pH unit intervals.



(a)

7.89	7.44	12.6	12.8	12.0	12.3	10.4	11.8	11.4	10.5
6.68					9.00				
6.44					10.2				10.0
6.78					11.6				9.22
8.00					10.0	8.78	11.6	11.0	10.4
9.44	10.0	12.6	13.0	11.6					10.0
7.44				13.0					7.89
6.68				8.78					7.44
6.78				7.44					10.5
9.67	11.4	12.1	11.8	10.0	11.0	8.00	12.0	7.89	9.44

(b)

Fig. 6. (a) Initial reaction time (defined as the time at which the intensity begins to increase) vs. bubble disappearance time (defined as the time at which the airbubble in the bead's storage cavity visually disappeared). (b) Air disappearance time at various locations in a  $10 \times 10$  array with reference to (a) (units are all in seconds).

underivatized or 'blank' bead (i.e., reference) in coordination with the values taken from an indicator bead. Here the  $A_R$ ,  $A_G$ , and  $A_B$  variables refer to the effective absorbance values at the three primary color ranges;  $I_{R,s}$ ,  $I_{G,s}$ , and  $I_{B,s}$  define the average raw light intensities for the three colors; and  $I_{R,o}$ ,  $I_{G,o}$ , and  $I_{B,o}$  refer to the average light intensities measured for the reference channels

$$A_R \approx -\log \left\{ \frac{I_{R,s}}{I_{R,o}} \right\}, \quad (9)$$

$$A_G \approx -\log \left\{ \frac{I_{G,s}}{I_{G,o}} \right\}, \quad (10)$$

$$A_B \approx -\log \left\{ \frac{I_{B,s}}{I_{B,o}} \right\}. \quad (11)$$

Using basic sensing scheme, Fig. 5b shows absorbance values of the alizarin complexone beads as the pH is varied over the range of 2–12 in one pH unit intervals. Goodey et al. (2001) described the actual chemical sensing for colorimetric detection well based on the microbead array. As shown in Fig. 6a, it was found that the time at which the color change begins does correlate very strongly with the time at which

the air in the bead's storage cavity visually disappeared. It is concluded for this specific case that the alizarin complexone beads started to respond very quickly when the sample fluid, first touched the beads. Fig. 6b shows air disappearance time at various locations in a  $10 \times 10$  array with reference to Fig. 6a. The test result show that the initial reaction time defined as the time at which onset of color change begins did not correlate strongly with the location in the array and the direction of fluid flow.

## 6. Conclusion

The development and initial characterization of a micro-machined fluidic structure for the introduction of liquid samples into a chip-based sensor composed of an array of polymeric microbeads has been presented. The structure consisted of a separately attached cover glass, a single silicon chip having micro-machined channels and microbead storage cavities, and a glass carrier. The device has been fabricated in a way to prevent exposure of receptors and indicator molecules from adverse conditions during chip fabrication.

One of the key parts of this system is a passive pump driven only by the capillary force, making the device simple and compact. The microfluidic structure was compatible with the basic sensing scheme for chemical detection requiring optical access through the microfluidic device. The velocity of penetration of a horizontal capillary for the device having a rectangular cross-section has been derived, and it is quite similar to the Washburn equation calculated for a pipe with a circular cross-section having uniform radius. A prediction of the derived equation compares well with the observed velocity. The flows of the fluid in the cavities are slightly different from each cavity and from chip to chip, and the average velocities of the fluid flow through the cavities are spread from cavity to cavity. This randomness is probably due to slightly different surface effects across the micromachined array generated during the chip fabrication. Absorbance values of the alizarin complexone beads were measured with the various pH using the basic sensing scheme. For a specific interaction between the alizarin complexone beads and pH 1 HCl solution, the alizarin complexone beads started to respond very quickly when the sample fluid first touched the beads. The system with simple fabrication procedure and the compact size of the microfluidic structure could be beneficial for a micro-total-analysis-system ( $\mu$ -TAS) and biomedical applications.

## Acknowledgement

Support for this project was provided by the National Institute of Health and Army Research Office MURI program (contract number DAAD 19-99-1-0207).

## References

- Abe, H., Esashi, M., Matsuo, T., 1979. ISFETs using inorganic gate thin films. *IEEE Trans. Electron. Devices* ED26, 1939–1944.
- Ali, M., Kirby, R., Goodey, A., Ellington, A., Neikirk, D.P., McDevitt, J.T., 2003. DNA hybridization and discrimination of single-nucleotide mismatches using microbead arrays. *Anal. Chem.* 75, 4732–4739.
- Arenkov, P., Kukhtin, A., Gemmel, A., Voloshchuk, S., Chupeeva, V., Mirzabekov, A., 2000. Protein microchips: use for immunoassay and enzymatic reactions. *Anal. Biochem.* 278, 123–131.
- Baltes, H., 1997. CMOS micro electro mechanical systems. *Sens. Mater.* 9, 331–346.
- Bodanszky, M., 1993. *Principles of Peptide Synthesis*, 2nd ed. Springer-Verlag, Berlin.
- Büttgenbach, S., Robohm, C., 1998. Microflow devices for miniaturized chemical analysis systems. In: *Proceedings of the SPIE Conference on Chemical Microsensors and Applications 3539*, Boston, MA, pp. 51–61.
- Christodoulides, N., Tran, M., Floriano, P.N., Rodriguez, M., Goodey, A., Ali, M., Neikirk, D., McDevitt, J.T., 2002. A microchip-based multianalyte assay system for the assessment of cardiac risk. *Anal. Chem.* 74, 3030–3036.
- Curey, T.E., Goodey, A., Tsao, A., Lavigne, J., Sohn, Y., McDevitt, J.T., Anslyn, E.V., Neikirk, D., Shear, J.B., 2001. Characterization of multicomponent monosaccharide solutions using an enzyme-based sensor array. *Anal. Biochem.* 293, 178–184.
- deMello, A., 2002. Plastic fantastic. *Lab on a Chip* 2, 31N–36N.
- Eaton, K., Douglas, B., Douglas, P., 2004. Luminescent oxygen sensors: time-resolved studies and modelling of heterogeneous oxygen quenching of luminescence emission from Pt and Pd octaethylporphyrins in thin polymer films. *Sens. Actuat. B* 97, 2–12.
- Feng, Y., Zhou, Z., Ye, X., Xiong, J., 2003. Passive valves based on hydrophobic microfluidics. *Sens. Actuat. A* 108, 138–143.
- Gardner, J.W., Bartlett, P.N., 1994. A brief history of electronic noses. *Sens. Actuat. B* 18, 211–220.
- Goodey, A., Lavigne, J., Savoy, S., Rodriguez, M., Theodore, C., Tsao, A., Simmons, G., Wright, J., Yoo, S.-J., Sohn, Y., Anslyn, E., Shear, J., Neikirk, D., McDevitt, J., 2001. Development of multianalyte sensor arrays composed of chemical derivatized polymeric microspheres localized in micromachined cavities. *J. Am. Chem. Soc.* 123, 2559–2570.
- Johnson, C.L., Wise, K.D., Schwank, J.W., 1988. A Thin-Film Gas Detector for Semiconductor Process gases. *Digest of the IEDM*, San Francisco, CA, p. 662.
- Kang, J., Kim, Y., Kim, H., Jeong, J., Park, S., 1997. Comfort sensing system for indoor environment. In: *Proceedings of the Transducers'97, the 1997 International Conference on Solid-State Sensors and Actuators*, vol. 1, Chicago, IL, pp. 311–314.
- Kim, C.-J., 2000. Microfluidic using the surface tension force in microscale. In: *Proceedings of the SPIE Conference on Microfluidic Devices and Systems III 4177*, Santa Clara, CA, pp. 49–54.
- Kondoh, J., Shiokawa, S., 1995. Liquid identification using SH-SAW sensors. In: *Proceedings of the Transducers'95, the Eighth International Conference on Solid-State Sensors and Actuators*, vol. 2, Stockholm, Sweden, pp. 716–719.
- Kovacs, G., 1998. *Micromachined Transducers Sourcebook*. McGraw-Hill, New York.
- Kugelmass, S.M., Lin, C., DeWitt, S.H., 1999. Fabrication and characterization of three-dimensional microfluidic arrays. In: *Proceedings of the SPIE Conference on Microfluidic Devices and Systems II 3877*, Santa Clara, CA, pp. 88–94.
- Lavigne, J.J., Savoy, S., Clevenger, M.B., Ritchie, J.E., McDoniel, B., Yoo, S.-J., Anslyn, E.V., McDevitt, J.T., Shear, J.B., Neikirk, D.P., 1998. Solution-based analysis of multiple analytes by a sensor array: toward the development of an 'electronic tongue'. *J. Am. Chem. Soc.* 120, 6429–6430.
- Lee, H.-S., Wang, S.S., Smolenski, D.J., Viola, M.B., Klusendorf, E.E., 1994. In situ monitoring of high-temperature degraded engine oil condition with microsensors. *Sens. Actuat. B* 20, 49–54.
- Lotierzo, M., Henry, O.Y.F., Piletsky, S., Tothill, I., Cullen, D., Kania, M., Hock, B., Turner, A.P.F., 2004. Surface plasmon resonance sensor for domoic acid based on grafted imprinted polymer. *Biosens. Bioelectron.* 20, 145–152.
- McCleskey, S.C., Griffin, M.J., Schneider, S.E., McDevitt, J.T., Anslyn, E.V., 2003. Differential receptors create patterns diagnostic for ATP and GTP. *J. Am. Chem. Soc.* 125, 1114–1115.
- Michael, K.L., Taylor, L.C., Schultz, S.L., Walt, D.R., 1998. Randomly ordered addressable high-density optical sensor arrays. *Anal. Chem.* 70, 1242–1248.
- Park, B.H., Park, Y.S., Sohn, Y.-S., Neikirk, D.P., 2003. Fabrication of bead size sorting chip for chemical array sensor. In: *Proceedings of the SPIE-Smart Sensors, Actuators, and MEMS*, Maspalomas, Gran Canaria, Spain, pp. 303–313.
- Petersen, K., 1996. *Biomedical Applications of MEMS*. *Digest of the IEDM*, San Francisco, CA, pp. 239–242.
- Puntambekar, A., Choi, J.-W., Ahn, C.H., Kim, S., Makhijani, V., 2002. Fixed-volume metering microdispenser module. *Lab on a Chip* 2, 213–218.
- Savoy, S., Lavigne, J.J., Yoo, S.-J., Wright, J., Rodriguez, M., Goodey, A., McDoniel, B., McDevitt, J.T., Anslyn, E.V., Shear, J.B., Ellington, A., Neikirk, D.P., 1998. Solution-based analysis of multiple analytes by a sensor array: toward the development of an "electronic tongue". In: *Proceedings of the SPIE Conference on Chemical Microsensors and Applications 3539*, Boston, MA, pp. 17–26.

- Sohn, Y.-S., Tsao, A., Anslyn, E., McDevitt, J., Shear, J.B., Neikirk, D.P., 2000. Liquid flow through an array-based chemical sensing system. In: Proceedings of the SPIE Conference on Microfluidic Devices and Systems III 4177, Santa Clara, CA, pp. 212–219.
- Washburn, E.D., 1921. The dynamics of capillary flow. *Phys. Rev.* 17, 273–283.
- Went, F.W., 1968. The size of man. *Am. Sci.* 56, 400–413.
- White, F.M., 1986. *Fluid Mechanics*, 2nd ed. McGraw-Hill, New York.
- Xu, H.X., Sha, M.Y., Wong, E.Y., Uphoff, J., Xu, Y.H., Treadway, J.A., Truong, A., O'Brien, E., Asquith, S., Stubbins, M., Spurr, N.K., Lai, E.H., Mahoney, W., 2003. Multiplexed SNP genotyping using the qbead system: a quantum dot-encoded microsphere-based assay. *Nucl. Acids Res.* 31, e43.